CHEMISTRY OF MATERIALS

pubs.acs.org/cm

Article

Structure and Stability of Core−Shell Cu−Pt Nanoparticles for Catalytic Applications

Alexandre C. Foucher, Daniel J. Rosen, Lucy K. Decker, Robert J. Macfarlane, Christopher B. Murray, Eric A. Stach, and Frances M. Ross*

Cite This: *Chem. Mater.* 2023, 35, 8758−8764

Read Online

ACCESS | Metrics & More | Article Recommendations | Supporting Information

ABSTRACT: We have successfully synthesized monodisperse core−shell Cu−Pt particles through a solvothermal method that enables control of the shell thickness to enhance the exposed Pt surface area and maintain a narrow size distribution. The core−shell Cu−Pt particles were tested as catalysts for the oxygen reduction reaction and showed promising catalytic properties. Postcatalysis analysis showed that most particles remain stable after catalysis. *In situ* electron microscopy demonstrates the remarkable stability of the sample in an oxidizing environment. It also visualizes the degradation mechanisms in oxidative conditions as being segregation of Pt and Cu oxide and the loss of the core−shell configuration. These core−shell Cu−Pt particles have the potential to improve the effectiveness of costly metals used in surface reactions for heterogeneous catalysis.

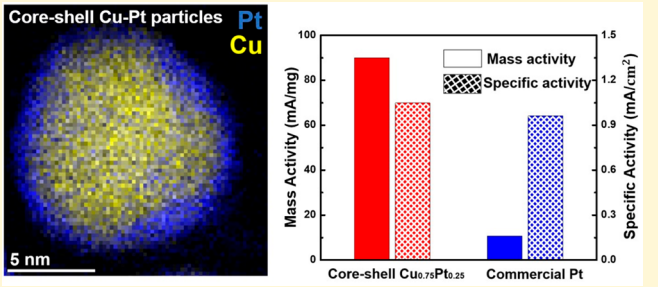

INTRODUCTION

Bimetallic nanoparticles have attracted significant interest in the fields of optics, electronics, and heterogeneous catalysis.[1−5] Metallic nanostructures composed of two elements permit a wider design space for controlling physical and chemical properties, as the morphology and composition of bimetallic nanostructures enables design variables not accessible to single-phase nanoparticles.[6−9] Core−shell nanoparticles in particular are increasingly explored due to several favorable properties.[10,11] Some studies have reported control over the optical properties of core−shell particles in solution, allowing the absorption spectrum to be modulated.[12,13] Other studies emphasize the potential applications in the fabrication of high-conductivity nanoparticle-based materials without the need for sintering of particles after deposition.[14,15] Finally, core−shell particles are of great interest for the surface reactions that underpin heterogeneous catalysis.[16−19] For instance, Pt nanoparticles are used for the oxygen reduction reaction (ORR) or hydrogen evolution reaction (HER)[20−24] but do not optimize each gram of Pt used in the structure. Instead, core−Pt-shell particles are ideal candidates for new catalyst development,[25,26] as they expose the maximum number of Pt atoms on the particle surface without making the particles so small that they become unstable in catalysis reaction conditions. Thus, the development of new synthesis methods to produce Pt-shell nanoparticles is a key area of investigation for heterogeneous catalyst research. In this work, we develop a route to form Cu−Pt nanoparticles and demonstrate the catalytic efficiency and stability of these structures, which feature active Pt shells surrounding cores of a more abundant and lower cost element.

MATERIALS AND METHODS

Synthesis. For the solvothermal synthesis, all materials were purchased from Sigma-Aldrich. The metal sources were Cu acetate ($Cu(OAc)_2 \geq 98\%$ purity) and Pt acetylacetonate ($Pt(acac)_2 \geq 97\%$ purity). Diphenyl ether (≥99% purity) was used as solvent and oleylamine (OLAM ≥ 90% purity) was used as capping agent. The synthesis method is based on an approach that has been described previously for other metallic particles.[27] For $Cu_{0.75}Pt_{0.25}$ particles, 14.5 mg of $Cu(OAc)_2$ and 20 mg of $Pt(acac)_2$ were dissolved in 20 mL of diphenyl ether and 25 mL of oleylamine in a 100 mL flask at room temperature. The mixture was stirred using a magnetic stir bar and placed under vacuum (<1 Torr) at a temperature of 95 °C for a period of 1 h to remove traces of water. The flask was then backfilled with (and kept under) nitrogen for the whole synthesis, and the temperature was rapidly elevated to 265 °C at a rate of 20 °C/min while stirring. The solution was kept at 265 °C for 50 min and then cooled under a nitrogen atmosphere (10 °C/min). The nanoparticles were isolated by adding hexane to decrease the viscosity of the solution and centrifuging the solution with a relative centrifugation force of 9016*g* for 5 min. After centrifugation, the remaining solution was transparent, with only minimal coloration from the remaining

Received: September 12, 2023
Revised: September 27, 2023
Published: October 12, 2023

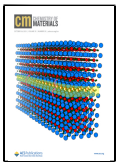

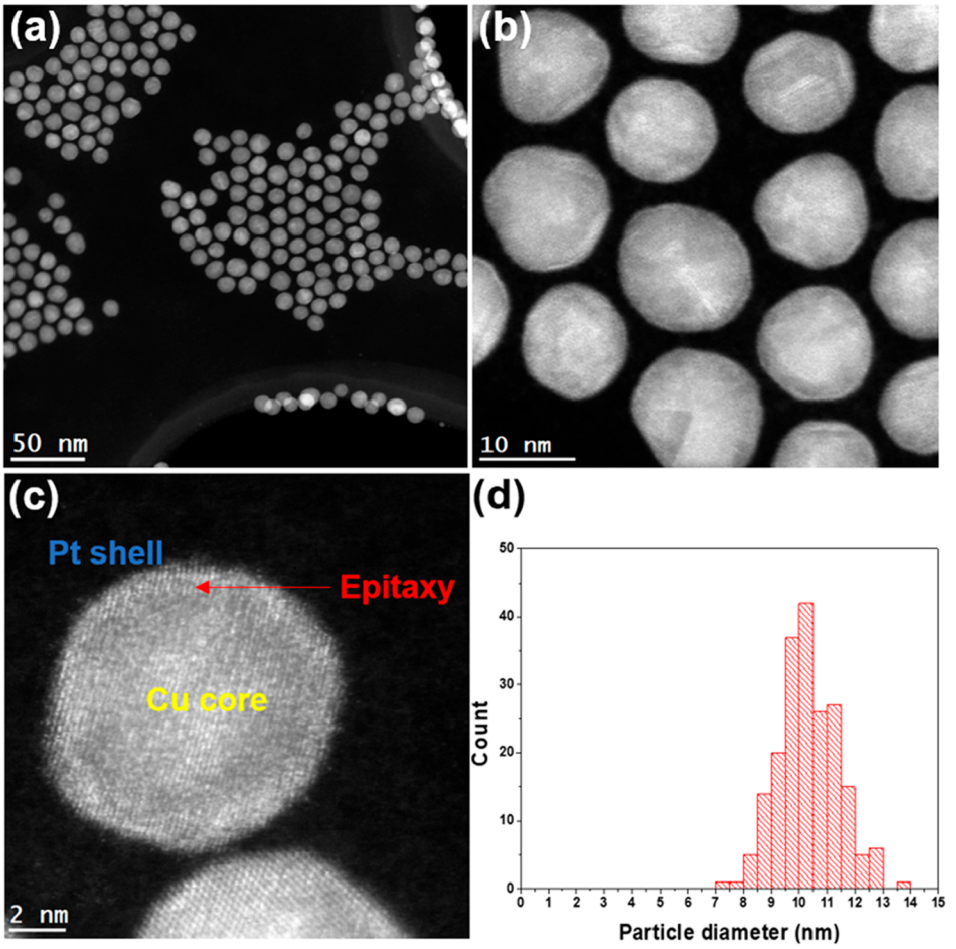

Figure 1. HAADF-STEM images and particle size distribution of $Cu_{0.75}Pt_{0.25}$ particles. (a) Low magnification image showing the narrow size distribution of the particles. (b) High magnification image. The particle to the right of the scale bar has a Cu core showing 5-fold twinning. (c) Atomically resolved HAADF-STEM image showing the epitaxial arrangement between the Pt shell and the Cu core. (d) Size distribution measured for 200 particles.

metallic precursors or unrecovered nanoparticles (Figure S1). The isolated particles were then redispersed in hexane for subsequent experiments. Similar synthetic protocols were used to prepare $Cu_{0.9}Pt_{0.1}$ and $Cu_{0.5}Pt_{0.5}$ core−shell particles; the quantities of precursors used to obtain these compositions are provided in Table S1. Additional details about the synthesis protocol are provided in the Supporting Information.

Characterization. The samples were imaged with a Hitachi HF5000-IS instrument operating at 200 kV. *Ex situ* and *in situ* imaging was performed on free-standing and supported Cu−Pt particles. For *in situ* analysis, the supported particles were deposited on a chip mounted on a dedicated holder for gas-heating analysis. Pure gases of H_2 and O_2 (purity >99.99%) were used and the pressure in the microscope was 8×10^{-2} Pa for both gases, with a mass flow of 3.5 sscm. EDS data were collected with detectors provided by Oxford Instruments (with Aztec software). EELS data (shown in Figure S2) were collected with a JEOL NEOARM instrument with a Gatan K2 Summit camera. For EELS measurements, the probe current was 500 pA, the camera length was 2 cm, and the condenser lens aperture had a diameter of 40 μm.

Electrochemical Analysis. Electrochemical measurements were performed using standard protocols.[29,30] Data were collected on a potentiostat (Epsilon, Bioanalytical Systems, Inc.) with a three-electrode system consisting of a glassy carbon working electrode (6 mm diameter), a Ag/AgCl reference electrode in 3 M KCl, and a Pt coil auxiliary electrode. The reaction took place in a one-compartment cell. All potentials collected during the testing were converted to a reversible hydrogen electrode (RHE). All samples were supported on amorphous carbon at 10% by weight. The catalyst ink was formed through sonication of water, isopropanol, and Nafion at a volume ratio of 4:1:0.01 and a nanocrystals (NC) on carbon concentration of 2 mg/mL. Ten μL of ink was deposited onto the working electrode at 100 rpm and dried under 700 rpm rotation. Cyclic voltammetry (CV) was taken in a range of 0.0−1.0 V vs RHE for ORR at a scan rate of 50 mV/s in N_2 saturated 0.1 M $HClO_4$. To test for stability, the samples were cycled between 0.6 and 1.0 V vs RHE in N_2 saturated 0.1 M $HClO_4$, with CV curves taken after 50 cycles at the beginning-of-life (BOL), 5000, 10 000, and 25 000 cycles. The electrochemically active surface area (ECSA) was determined by using hydrogen underpotential deposition measurements. Linear sweep voltammetry (LSV) was taken at 1600 rpm from 0.0 to 1.0 V vs RHE. IR compensation was performed by using the automatic feature of the potentiostat. The mass activity was normalized by the Pt mass determined from ICP-OES, and the specific activity was normalized by ECSA.

RESULTS AND DISCUSSION

The as-synthesized nanoparticles were studied by *ex situ* scanning transmission electron microscopy (STEM). Figure 1 shows high-angle annular dark-field (HAADF)-STEM images of $Cu_{0.75}Pt_{0.25}$ and the corresponding size distribution from the analysis of >200 particles. Electron energy-loss spectroscopy (EELS) measurements, provided in Figure S2, show that Cu is

https://doi.org/10.1021/acs.chemmater.3c02334
Chem. Mater. 2023, 35, 8758−8764

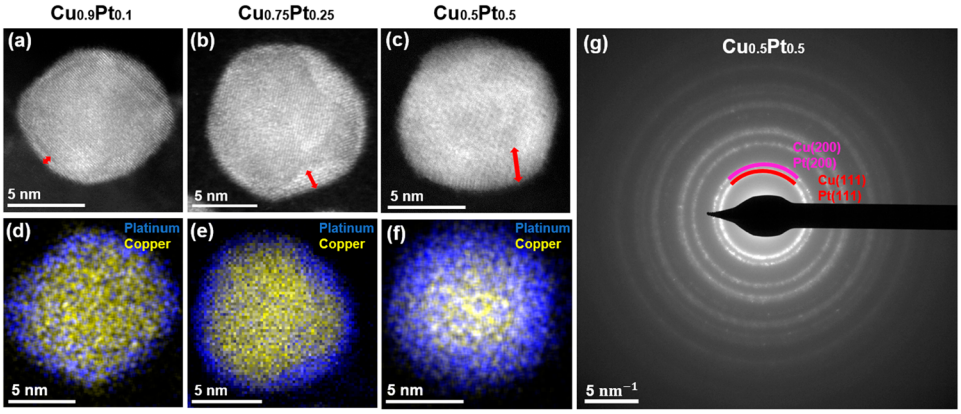

Figure 2. Typical HAADF-STEM images and EDS maps for $Cu_{0.90}Pt_{0.10}$, $Cu_{0.75}Pt_{0.25}$, and $Cu_{0.50}Pt_{0.50}$. (a–c) High magnification of single particles. (d–f) Corresponding EDS maps. The Pt shell thickness depends on the Cu:Pt ratio. (g) Electron diffraction pattern showing the FCC crystal structures of Pt and Cu.

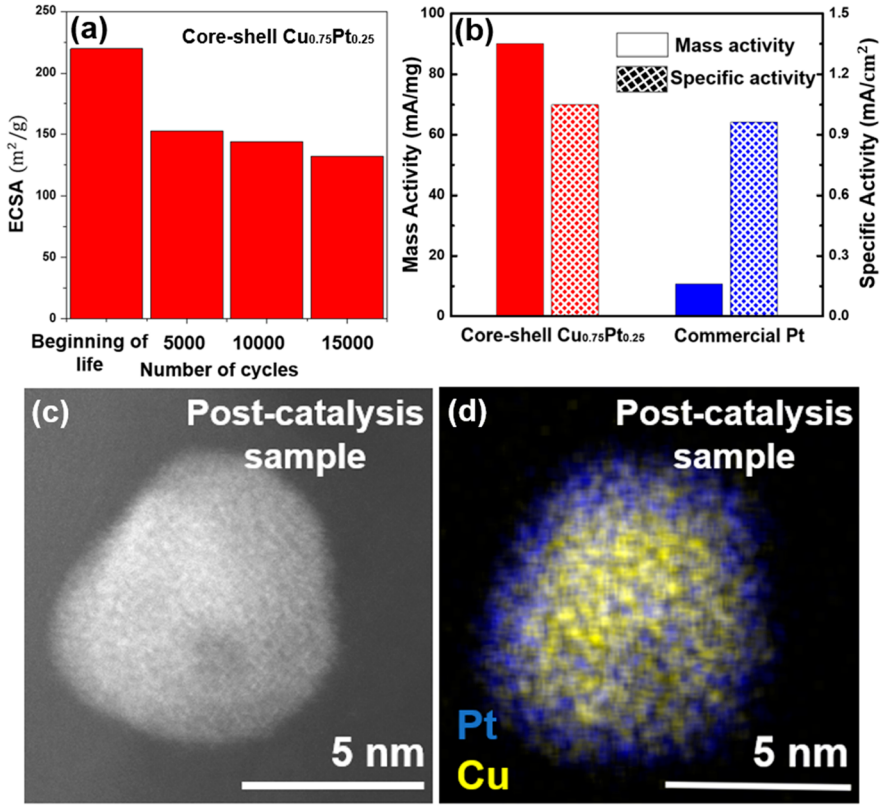

Figure 3. Investigation of the catalytic properties of core–shell $Cu_{0.75}Pt_{0.25}$ particles for ORR in an acidic environment. (a) ECSA of fresh samples and after many cycles. The catalyst displays good stability. (b) Measurement of mass activity and specific activity (hatched) of $Cu_{0.75}Pt_{0.25}$ core–shell particles compared to a commercial Pt catalyst. (c) Postcatalysis sample after 15000 cycles. For most particles, the core–shell configuration was not changed. (d) Combined EDS map of particle seen in (c) showing that Pt remains on the surface and Cu remains in the core.

not substantially oxidized in the fresh samples and the size distribution of the particles is tightly controlled (9.9 ± 1.2 nm). We anticipate that the formation pathway of these core–shell particles is similar to the process that has previously been described[27] for similar bimetallic core–shell nanoparticles with a Cu interior: Cu–Ru, Cu–Rh, and Cu–Ir. Thus, we hypothesize that the first event in the core–shell synthesis is the nucleation of Cu particles after the temperature is increased, which can be seen by a change in color of the solution at around 180 °C. Once the solution reaches 265 °C, the Pt precursor, which is more difficult to reduce, slowly coalesces on the surface of the Cu particles, forming a shell of Pt. Control over the size distribution is, therefore, mostly determined by the size of the initial Cu particles. Hence, a rapid increase in the temperature (at least 15–20 °C/min) is necessary to obtain a monodisperse size distribution. Additionally, one can notice that many particles are polycrystalline, with some particles having an icosahedral configuration, as seen in Figure 1b. Finally, a close look at atomic-scale images (Figure 1c) shows an epitaxial arrangement between the Pt shell and Cu core with no visible dislocations at the interface between the two metals.

https://doi.org/10.1021/acs.chemmater.3c02334
Chem. Mater. 2023, 35, 8758–8764

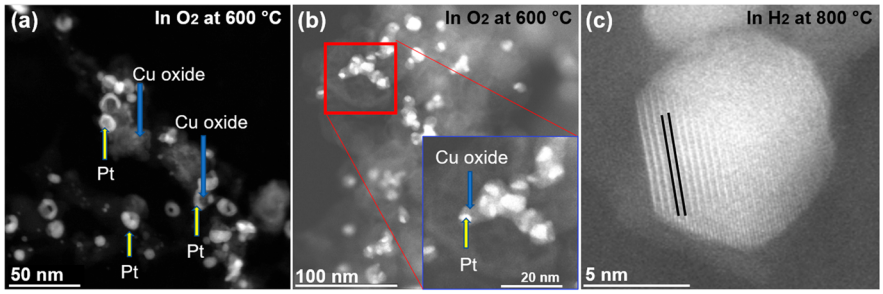

Figure 4. *In situ* STEM analysis in 5×10^{-2} Pa of gases to evaluate the stability of core−shell $Cu_{0.75}Pt_{0.25}$ particles. (a, b) HAADF-STEM images of the sample after exposure to O_2 at 600 °C showing that the core−shell configuration is progressively lost and Pt and CuO become segregated. (c) Sample with a Cu:Pt ratio of 1:1 after annealing in H_2 at 800 °C for 30 min showing formation of an intermetallic phase (black lines).

The segregation of Pt at the surface is confirmed by energy-dispersive X-ray spectroscopy (EDS) maps of the Cu K and Pt L edges (Figure 2). Surface segregation of Pt is initially surprising, given that Pt and Cu are known to be miscible.[28] This suggests that the formation of these core−shell Cu−Pt particles is dominated by synthesis kinetics and that the process is both too short and at too low a temperature to permit large amounts of migration of the comparatively larger Pt atoms into the Cu core. A control experiment to verify this hypothesis was performed by trying to synthesize core−shell Cu−Pd particles with the same method (recipe details are in the Supporting Information, Figure S3). For this metal pair, which is also expected to be miscible,[29] Pd fully mixed with Cu and formed a random alloy phase, and not a core−shell structure. This is consistent with the prediction that the smaller size of Pd atoms (van der Waals radius of 163 pm) compared to Pt atoms (radius of 175 pm) allows more rapid diffusion into the Cu lattice (atomic radius of 128 pm) so that the thermodynamically preferred intermixing can occur during the time of the synthesis. Additionally, the reactivities of Pd and Pt precursors are not similar, which may also explain the differences in Cu−Pd and Cu−Pt particles. One can assume that the higher decomposition temperature of $Pt(acac)_2$ is beneficial for the formation of core−shell Cu−Pt particles. As the temperature of the solution is increased, Cu cores are formed at low temperatures (around 230 °C) and Pt atoms coalesce on the surface of Cu at high temperatures (around 250 °C). In contrast, the reactivity of $Pd(acac)_2$ is lower, which causes the aggregation of Cu and Pd at the same temperature, causing the formation of an alloyed Cu−Pd phase instead of a core−shell structure.

We have examined the properties of these nanoparticles by carrying out syntheses with different Pt−Cu ratios. We find that the diffraction patterns are consistent with a face-centered cubic (FCC) structure for Pt and Cu (Figure 2g). An investigation of the diffraction patterns and atomic-scale image did not show any signs of strain in the Cu or Pt lattice. The measured thickness of the Pt shell is consistent with the theoretical thickness calculated for the ratio of precursors Cu:Pt used in the recipe: the theoretical Pt thickness should be 9% of the radius of the Cu core in $Cu_{0.9}Pt_{0.1}$, 23% in $Cu_{0.75}Pt_{0.25}$ and 53% in $Cu_{0.5}Pt_{0.5}$. This shows the benefit of the synthesis process in controlling the shell thickness; different catalytic conditions may benefit from either thicker shells (to enhance particle stability under harsher conditions) or thinner shells (to maximize the Pt efficiency). Thus, the design of Cu−Pt core−shells shown in this work is flexible, with control over the size, shape, and thickness of the Pt shell.

To examine their catalytic efficiency and stability, $Cu_{0.75}Pt_{0.25}$ particles supported on amorphous carbon were calcinated to remove ligands (details in Supporting Information) and tested as a catalyst for the ORR in an acidic medium. Particles were deposited on carbon support with a 10% weight loading of Pt, and their catalytic behavior was compared to the results of a commercial Pt nanoparticle catalyst reported in a previous publication.[30] The commercial Pt catalyst contained 3 nm Pt particles supported on carbon and was tested with the same protocol as that used in this work. The electrochemically active surface area (ECSA) of the Pt−Cu core−shell particles developed here is very high (above 200 m^2/g) and superior to many Pt-based catalysts reported in previous investigations (Figure 3).[31] Activity data were taken at a potential of 0.9 V vs RHE. Linear sweep voltammetry (LSV) and the cycling voltammetry (CV) data at the beginning of life (BOL) are also provided in Figure S4. Additionally, the core−shell $Cu_{0.75}Pt_{0.25}$ has a superior mass and specific activity than the commercial Pt catalysis (Figure 3b), making it a promising candidate to expand the range of nanomaterials to further optimize the ORR in fuel cells. Most interestingly, the system has very good stability, as the ECSA remains above 120 m^2/g after 15000 cycles. This is consistent with *in situ* STEM images of the particles postcatalysis, which show that the core−shell configuration can resist these strongly oxidative environments (Figure 3c,d). In most cases (63% of particles), the core−shell configuration was preserved (Figure S5); the remaining particles tended to exhibit more dramatic changes where Cu and Pt formed a mixed solution (Figures S6 and S7). No thick Cu oxide layer was observed to envelop the active Pt, as has sometimes been observed in bimetallic samples with an element that easily oxidizes and segregates to the surface.[32]

To expand the investigation of the stability of the particles and thus their utility to catalyze other reactions, an *in situ* STEM experiment was performed under a gaseous environment and elevated temperature using a Hitachi HF5000-IS environmental transmission electron microscope (Figure 4). The pressure was 8×10^{-2} Pa for the whole experiment and for all gases. $Cu_{0.75}Pt_{0.25}$ particles were deposited on an amorphous carbon support on an *in situ* TEM chip capable of elevated temperatures via an encapsulated patterned Pt Joule heater. The $Cu_{0.75}Pt_{0.25}$ particles were stable in O_2 at temperatures up to 450 °C, as the thick Pt shells prevent oxidation of the Cu core (Figure S8). This is notable as Cu tends to oxidize easily, and bimetallic particles with Cu are not generally stable in an oxidative atmosphere.[33] Above 450 °C, prolonged exposure to an O_2-rich environment leads to the oxidation of the Cu core into CuO, as shown by EELS of the

https://doi.org/10.1021/acs.chemmater.3c02334
Chem. Mater. 2023, 35, 8758−8764

Cu $L_{2,3}$ edge. We observed segregation of Pt and CuO (Figure 4a,b), with a progressive disruption of the Pt shell (Figure 4a). It was possible to observe Janus CuO-Pt particles after prolonged exposure (Figure 4b, at least 30 min of exposure). However, CuO did not cover the Pt, which indicates that Pt could still act as a catalyst. It is also interesting to observe that core−shell Cu−Pt particles do not behave in the same way as core−shell Cu−Ir particles, which have been described previously.[34,27] In those reports, the Ir shell is stable even if the Cu core oxidizes, perhaps due to the higher melting point of Ir (2,446 °C for Ir vs 1768 °C for Pt). Also, Pt is also prone to sintering and migration on a support, which may reduce the stability of the structure.[35−37] Nevertheless, the catalytic testing and the *in situ* experiments underline the promising overall stability of core−shell Cu−Pt particles provided that the temperature remains below a limit (which in our *in situ* experiment was 450 °C, still relevant for many catalytic processes).[26,38]

If $Cu_{0.75}Pt_{0.25}$ particles are exposed to H_2 at elevated temperatures (Figure 4c), the core−shell configuration is partly converted into an intermetallic CuPt phase with a Cu:Pt ratio of (1:1), consistent with other investigations of Cu−Pt particles.[26] Atomic resolution imaging shows atomic rows with high brightness (Pt atoms) and low brightness (Cu), typical for an intermetallic phase with a 1:1 ratio between the two metals. Excess Cu can be found on the surface of the carbon support. Hence, the Cu−Pt particles can be thermally treated with O_2 or H_2 to obtain new morphologies tailored to the potential applications.

This work underlines that core−shell Cu−Pt particles can be obtained in an approach similar to the synthesis of Cu−Ru. Cu−Rh and Cu−Ir particles shown in a previous work.[27] The reported synthesis method of core−shell Cu−Pt in this work is flexible and efficient and can be adapted for many potential applications. The particle size distribution is narrow, and the thickness of the Pt shell can be controlled by the amount of the Pt precursor used for synthesis. Electrochemical testing of $Cu_{0.75}Pt_{0.25}$ for ORR shows promising results in terms of stability and activity, with the preservation of the core−shell configuration for most particles. *In situ* STEM analysis showed that the particles are stable in some oxidative conditions as the Pt shells prevent the oxidation of the Cu core. Thus, these core−shell Cu−Pt particles can be of great interest for the design of highly active and stable nanocatalysts and can help to reduce the amount of expensive Pt needed for catalysis.

■ ASSOCIATED CONTENT

Supporting Information

The Supporting Information is available free of charge at https://pubs.acs.org/doi/10.1021/acs.chemmater.3c02334.

Additional STEM images, EELS, size distribution histograms, and raw electrochemical data (PDF)

■ AUTHOR INFORMATION

Corresponding Author

Frances M. Ross − *Department of Materials Science and Engineering, Massachusetts Institute of Technology, Cambridge, Massachusetts 02139, United States;* orcid.org/0000-0003-0838-9770; Email: fmross@mit.edu

Authors

Alexandre C. Foucher − *Department of Materials Science and Engineering, Massachusetts Institute of Technology, Cambridge, Massachusetts 02139, United States;* orcid.org/0000-0001-5042-4002

Daniel J. Rosen − *Department of Materials Science and Engineering, University of Pennsylvania, Philadelphia, Pennsylvania 19104, United States;* orcid.org/0000-0003-1463-7363

Lucy K. Decker − *Department of Materials Science and Engineering, University of Pennsylvania, Philadelphia, Pennsylvania 19104, United States*

Robert J. Macfarlane − *Department of Materials Science and Engineering, Massachusetts Institute of Technology, Cambridge, Massachusetts 02139, United States;* orcid.org/0000-0001-9449-2680

Christopher B. Murray − *Department of Materials Science and Engineering and Department of Chemistry, University of Pennsylvania, Philadelphia, Pennsylvania 19104, United States*

Eric A. Stach − *Department of Materials Science and Engineering and Laboratory for Research on the Structure of Matter, University of Pennsylvania, Philadelphia, Pennsylvania 19104, United States;* orcid.org/0000-0002-3366-2153

Complete contact information is available at: https://pubs.acs.org/10.1021/acs.chemmater.3c02334

Notes

The authors declare no competing financial interest.

■ ACKNOWLEDGMENTS

This work was funded in part by Semiconductor Research Corporation (SRC). This work was supported by the Office of Naval Research (ONR) MURI through Grant No. N00014-17-1-2661. This work was carried out with the use of facilities and instrumentation supported by NSF through the Massachusetts Institute of Technology Materials Research Science and Engineering Center DMR - 1419807. This project was carried out in part through the use of MIT.nano's facilities. This work was also supported as part of the Integrated Mesoscale Architectures for Sustainable Catalysis (IMASC), an Energy Frontier Research Center funded by the U.S. Department of Energy, Office of Science, Basic Energy Sciences under Award #DE-SC0012573. This work was carried out in part at the Singh Center for Nanotechnology, which is supported by the NSF National Nanotechnology Coordinated Infrastructure Program under grant NNCI-2025608. Additional support to the Nanoscale Characterization Facility at the Singh Center has been provided by the Laboratory for Research on the Structure of Matter (MRSEC) supported by the National Science Foundation (DMR-1720530).

■ REFERENCES

(1) Wang, Y.; Yang, Y.; Jia, S.; Wang, X.; Lyu, K.; Peng, Y.; Zheng, H.; Wei, X.; Ren, H.; Xiao, L.; Wang, J.; Muller, D. A.; Abruña, H. D.; Hwang, B. J.; Lu, J.; Zhuang, L. Synergistic Mn-Co Catalyst Outperforms Pt on High-Rate Oxygen Reduction for Alkaline Polymer Electrolyte Fuel Cells. *Nat. Commun.* **2019**, *10*, 1506.

(2) Luneau, M.; Guan, E.; Chen, W.; Foucher, A. C.; Marcella, N.; Shirman, T.; Verbart, D. M. A.; Aizenberg, J.; Aizenberg, M.; Stach, E. A.; Madix, R. J.; Frenkel, A. I.; Friend, C. M. Enhancing Catalytic

Performance of Dilute Metal Alloy Nanomaterials. *Commun. Chem.* **2020**, *3*, 46.
(3) Garfinkel, D. A.; Pakeltis, G.; Tang, N.; Ivanov, I. N.; Fowlkes, J. D.; Gilbert, D. A.; Rack, P. D. Optical and Magnetic Properties of Ag-Ni Bimetallic Nanoparticles Assembled via Pulsed Laser-Induced Dewetting. *ACS Omega* **2020**, *5*, 19285−19292.
(4) Zaleska-Medynska, A.; Marchelek, M.; Diak, M.; Grabowska, E. Noble Metal-Based Bimetallic Nanoparticles: The Effect of the Structure on the Optical, Catalytic and Photocatalytic Properties. *Adv. Colloid Interface Sci.* **2016**, *229*, 80−107.
(5) Tahsini, N.; Yang, A. C.; Streibel, V.; Werghi, B.; Goodman, E. D.; Aitbekova, A.; Bare, S. R.; Li, Y.; Abild-Pedersen, F.; Cargnello, M. Colloidal Platinum-Copper Nanocrystal Alloy Catalysts Surpass Platinum in Low-Temperature Propene Combustion. *J. Am. Chem. Soc.* **2022**, *144*, 1612−1621.
(6) van der Hoeven, J. E. S.; Jelic, J.; Olthof, L. A.; Totarella, G.; van Dijk-Moes, R. J. A.; Krafft, J.-M.; Louis, C.; Studt, F.; van Blaaderen, A.; de Jongh, P. E. Unlocking Synergy in Bimetallic Catalysts by Core−Shell Design. *Nat. Mater.* **2021**, *20*, 1216−1220.
(7) Wu, C. H.; Liu, C.; Su, D.; Xin, H. L.; Fang, H.-T.; Eren, B.; Zhang, S.; Murray, C. B.; Salmeron, M. B. Bimetallic Synergy in Cobalt−Palladium Nanocatalysts for CO Oxidation. *Nat. Catal.* **2019**, *2*, 78−85.
(8) Foucher, A. C.; Marcella, N.; Lee, J. D.; Tappero, R.; Murray, C. B.; Frenkel, A. I.; Stach, E. A. Dynamical Change of Valence States and Structure in $NiCu_3$ Nanoparticles during Redox Cycling. *J. Phys. Chem. C* **2022**, *126*, 1991−2002.
(9) Luneau, M.; Shirman, T.; Foucher, A. C.; Duanmu, K.; Verbart, D. M. A.; Sautet, P.; Stach, E. A.; Aizenberg, J.; Madix, R. J.; Friend, C. M. Achieving High Selectivity for Alkyne Hydrogenation at High Conversions with Compositionally Optimized PdAu Nanoparticle Catalysts in Raspberry Colloid-Templated SiO_2. *ACS Catal.* **2020**, *10*, 441−450.
(10) Yoon, D.; Bang, S.; Park, J.; Kim, J.; Baik, H.; Yang, H.; Lee, K. One Pot Synthesis of Octahedral {111} CuIr Gradient Alloy Nanocrystals with a Cu-Rich Core and an Ir-Rich Surface and Their Usage as Efficient Water Splitting Catalyst. *CrystEngComm* **2015**, *17*, 6843−6847.
(11) Dai, S.; Chou, J. P.; Wang, K. W.; Hsu, Y. Y.; Hu, A.; Pan, X.; Chen, T. Y. Platinum-Trimer Decorated Cobalt-Palladium Core-Shell Nanocatalyst with Promising Performance for Oxygen Reduction Reaction. *Nat. Commun.* **2019**, *10*, 440.
(12) Nasilowski, M.; Nienhaus, L.; Bertram, S. N.; Bawendi, M. G. Colloidal Atomic Layer Deposition Growth of PbS/CdS Core/Shell Quantum Dots. *Chem. Commun.* **2017**, *53*, 869−872.
(13) Hansen, E. C.; Bertram, S. N.; Yoo, J. J.; Bawendi, M. G. Zinc Thiolate Enables Bright Cu-Deficient Cu-In-S/ZnS Quantum Dots. *Small* **2019**, *15*, 1901462.
(14) Zhang, W.; Zhou, Y.; Ding, Y.; Song, L.; Yuan, Q.; Zhao, W.; Xu, C.; Wei, J.; Li, M.; Ji, H. Sintering Mechanism of Size-Controllable Cu-Ag Core−Shell Nanoparticles for Flexible Conductive Film with High Conductivity, Antioxidation, and Electrochemical Migration Resistance. *Appl. Surf. Sci.* **2022**, *586*, 152691.
(15) Fang, Y.; Zeng, X.; Chen, Y.; Ji, M.; Zheng, H.; Xu, W.; Peng, D. L. Cu@Ni Core−Shell Nanoparticles Prepared via an Injection Approach with Enhanced Oxidation Resistance for the Fabrication of Conductive Films. *Nanotechnology* **2020**, *31*, 355601.
(16) Ding, Y.; Fan, F.; Tian, Z.; Wang, Z. L. Atomic Structure of Au-Pd Bimetallic Alloyed Nanoparticles. *J. Am. Chem. Soc.* **2010**, *132*, 12480−12486.
(17) Szabat, H.; Pawłowski, J.; Połczyński, P.; Jurczakowski, R. Shell Tailoring of Core−Shell Nanoparticles for Heterogeneous Catalysis. *Electrochem. commun.* **2021**, *128*, 107055.
(18) Xin, H. L.; Alayoglu, S.; Tao, R.; Genc, A.; Wang, C. M.; Kovarik, L.; Stach, E. A.; Wang, L. W.; Salmeron, M.; Somorjai, G. A.; Zheng, H. Revealing the Atomic Restructuring of Pt-Co Nanoparticles. *Nano Lett.* **2014**, *14*, 3203−3207.
(19) Xie, M.; Lyu, Z.; Chen, R.; Shen, M.; Cao, Z.; Xia, Y. Pt-Co@Pt Octahedral Nanocrystals: Enhancing Their Activity and Durability toward Oxygen Reduction with an Intermetallic Core and an Ultrathin Shell. *J. Am. Chem. Soc.* **2021**, *143*, 8509−8518.
(20) Yu, Z.; Zhang, J.; Liu, Z.; Ziegelbauer, J. M.; Xin, H.; Muller, D. A.; Wagner, F. T.; Dutta, I. Comparison between Dealloyed $PtCo_3$ and $PtCu_3$ Cathode Catalysts for Proton Exchange Membrane Fuel Cells. *J. Phys. Chem. C* **2012**, *116*, 19877−19885.
(21) Ge, X.; Sumboja, A.; Wuu, D.; An, T.; Li, B.; Goh, F. W. T.; Hor, T. S. A.; Zong, Y.; Liu, Z. Oxygen Reduction in Alkaline Media: From Mechanisms to Recent Advances of Catalysts. *ACS Catal.* **2015**, *5*, 4643−4667.
(22) Jiang, K.; Liu, B.; Luo, M.; Ning, S.; Peng, M.; Zhao, Y.; Lu, Y.-R.; Chan, T.-S.; de Groot, F. M. F.; Tan, Y. Single Platinum Atoms Embedded in Nanoporous Cobalt Selenide as Electrocatalyst for Accelerating Hydrogen Evolution Reaction. *Nat. Commun.* **2019**, *10*, 1743.
(23) Garlyyev, B.; Kratzl, K.; Rück, M.; Michalička, J.; Fichtner, J.; Macak, J. M.; Kratky, T.; Günther, S.; Cokoja, M.; Bandarenka, A. S.; Gagliardi, A.; Fischer, R. A. Optimizing the Size of Platinum Nanoparticles for Enhanced Mass Activity in the Electrochemical Oxygen Reduction Reaction. *Angew. Chemie Int. Ed.* **2019**, *58*, 9596−9600.
(24) Cheng, N.; Stambula, S.; Wang, D.; Banis, M. N.; Liu, J.; Riese, A.; Xiao, B.; Li, R.; Sham, T. K.; Liu, L. M.; Botton, G. A.; Sun, X. Platinum Single-Atom and Cluster Catalysis of the Hydrogen Evolution Reaction. *Nat. Commun.* **2016**, *7*, 13628.
(25) Wang, D.; Xin, H. L.; Hovden, R.; Wang, H.; Yu, Y.; Muller, D. A.; DiSalvo, F. J.; Abruña, H. D. Structurally Ordered Intermetallic Platinum−Cobalt Core−Shell Nanoparticles with Enhanced Activity and Stability as Oxygen Reduction Electrocatalysts. *Nat. Mater.* **2013**, *12*, 81−87.
(26) Foucher, A. C.; Yang, S.; Rosen, D. J.; Huang, R.; Pyo, J. B.; Kwon, O.; Owen, C. J.; Sanchez, D. F.; Sadykov, I. I.; Grolimund, D.; Kozinsky, B.; Frenkel, A. I.; Gorte, R. J.; Murray, C. B.; Stach, E. A. Synthesis and Characterization of Stable Cu-Pt Nanoparticles under Reductive and Oxidative Conditions. *J. Am. Chem. Soc.* **2023**, *145*, 5410−5421.
(27) Foucher, A. C.; Yang, S.; Rosen, D. J.; Lee, J. D.; Huang, R.; Jiang, Z.; Barrera, F. G.; Chen, K.; Hollyer, G. G.; Friend, C. M.; Gorte, R. J.; Murray, C. B.; Stach, E. A. Synthesis and Characterization of Core-Shell Cu-Ru, Cu-Rh, and Cu-Ir Nanoparticles. *J. Am. Chem. Soc.* **2022**, *144*, 7919−7928.
(28) Yang, C.; Ko, B. H.; Hwang, S.; Liu, Z.; Yao, Y.; Luc, W.; Cui, M.; Malkani, A. S.; Li, T.; Wang, X.; Dai, J.; Xu, B.; Wang, G.; Su, D.; Jiao, F.; Hu, L. Overcoming Immiscibility toward Bimetallic Catalyst Library. *Sci. Adv.* **2020**, *6*, eaaz6844.
(29) Xie, W.; Zhang, G.; Guo, Z.; Huang, H.; Ye, J.; Gao, X.; Yue, K.; Wei, Y.; Zhao, L. Shape-Controllable and Kinetically Miscible Copper−Palladium Bimetallic Nanozymes with Enhanced Fenton-like Performance for Biocatalysis. *Mater. Today Bio* **2022**, *16*, 100411.
(30) Rosen, D. J.; Foucher, A. C.; Lee, J. D.; Yang, S.; Marino, E.; Stach, E. A.; Murray, C. B. Microwave Heating of Nanocrystals for Rapid, Low-Aggregation Intermetallic Phase Transformations. *ACS Mater. Lett.* **2022**, *4*, 823−830.
(31) Garsany, Y.; Ge, J.; St-Pierre, J.; Rocheleau, R.; Swider-Lyons, K. E. Analytical Procedure for Accurate Comparison of Rotating Disk Electrode Results for the Oxygen Reduction Activity of Pt/C. *J. Electrochem. Soc.* **2014**, *161*, F628−F640.
(32) Foucher, A. C.; Marcella, N.; Lee, J. D.; Rosen, D. J.; Tappero, R.; Murray, C. B.; Frenkel, A. I.; Stach, E. A. Structural and Valence State Modification of Cobalt in CoPt Nanocatalysts in Redox Conditions. *ACS Nano* **2021**, *15*, 20619−20632.
(33) Foucher, A. C.; Marcella, N.; Lee, J. D.; Tappero, R.; Murray, C. B.; Frenkel, A. I.; Stach, E. A. Dynamical Change of Valence States and Structure in $NiCu_3$ Nanoparticles during Redox Cycling. *J. Phys. Chem. C* **2022**, *126*, 1991−2002.
(34) Foucher, A. C.; Rosen, D. J.; Yang, S.; Ferreira Sanchez, D.; Sadykov, I.; Grolimund, D.; Frenkel, A. I.; Murray, C. B.; Stach, E. A. Stable and Efficient Ir Nanoshells for Oxygen Reduction and Evolution Reactions. *Chem. Mater.* **2023**, *35*, 4572−4580.

(35) Harris, P. J. F. The Sintering of Platinum Particles in an Alumina-Supported Catalyst: Further Transmission Electron Microscopy Studies. *J. Catal.* **1986**, *97*, 527−542.
(36) Mao, X.; Foucher, A. C.; Montini, T.; Stach, E. A.; Fornasiero, P.; Gorte, R. J. Epitaxial and Strong Support Interactions between Pt and $LaFeO_3$ Films Stabilize Pt Dispersion. *J. Am. Chem. Soc.* **2020**, *142*, 10373−10382.
(37) Borgna, A.; Le Normand, F.; Garetto, T.; Apesteguia, C. R.; Moraweck, B. Sintering of Pt/Al_2O_3 Reforming Catalysts: EXAFS Study of the Behavior of Metal Particles under Oxidizing Atmosphere. *Catal. Lett.* **1992**, *13*, 175−188.
(38) Foucher, A. C.; Marcella, N.; Lee, J. D.; Rosen, D. J.; Tappero, R.; Murray, C. B.; Frenkel, A. I.; Stach, E. A. Structural and Valence State Modification of Cobalt in CoPt Nanocatalysts in Redox Conditions. *ACS Nano* **2021**, *15*, 20619−20632.

https://doi.org/10.1021/acs.chemmater.3c02334
Chem. Mater. 2023, 35, 8758−8764